



Shear Behaviour of Rock–Tailings Backfill Interface: Effect of Cementation, Rock Type, and Rock Surface Roughness

Kun Fang · Mamadou Fall

Received: 22 June 2020 / Accepted: 25 September 2020 / Published online: 20 October 2020
© Springer Nature Switzerland AG 2020

Abstract Determination of interface shear behaviour is critical for the design of many geotechnical structures, including cemented paste backfill structures. However, the shear characteristics of the CPB–rock interface is not fully understood. No studies have been conducted to assess the impact of the characteristics of rock (e.g., type of rock, rock surface roughness), cementation and the coupled effects of surface roughness and degree of cementation on the shear characteristics of the interface between rock and tailings backfill. This paper presents new findings of research conducted to investigate the effect of different types of rock, rock surface roughness and degree of cementation as well as the coupled effects of these factors on the shear properties and behaviour of the interface between cemented paste backfill (CPB) and rock. The results show that roughness and the interaction between roughness and degree of cement hydration have a significant effect on the shear characteristics of a CPB–rock interface. For a certain degree of cementation, the roughness can increase the shear strength due to the increased size of the interlocking structure. The interface samples with roughness, especially those sheared at high normal stress, tend to experience two peak shear stresses during the shear test. Moreover, the shear strength,

shear dilation, and adhesion of the interface also increase with degree of cementation. However, according to the revised Barton's equation, the effective friction angle of interface with roughness experiences a decreasing tendency with degree of cementation, despite the increasing tendency of the friction angle of the smooth interface. In other words, the interface asperity contributes more to the evolution of adhesion, and the contribution of friction angle to the shear strength is partially offset. It is also found that the rock type (considered in this study) has limited effects on the interface shear properties. The failure of the interface between CPB and rock is because of the existence of the interfacial transition zone, which is characterized by high porosity. These new findings have practical importance to the design of the underground CPB structures.

Keywords Rock · Interface · Tailings · Cemented paste backfill · Shear strength · Mine

1 Introduction

Mining is a key contributor to the economy of many countries in the world. It provides society with the mineral raw materials that are essential for the construction and high-tech sectors, industrial production, agriculture, the transport and communication sectors, and merchandise producers (Roshani et al.

K. Fang · M. Fall (✉)
Department of Civil Engineering, University of Ottawa,
161 Colonel by, Ottawa, ON K1N 6N5, Canada
e-mail: mfall@uottawa.ca

2017). However, underground mining activities are associated with numerous geotechnical hazards that pose a serious threat to the health and safety not only of mine workers, but also of communities living near mines (Hassani and Archibald 1998; Fall et al. 2009). These hazards include: (1) mining subsidence, (2) underground mine voids (stopes) collapse or failure, (3) rockbursts, (4) ground fissures due to underground mining, (5) tailings dam failure and/or acid mine drainage due to the improper management of mine wastes, etc. Moreover, due to the gradual depletion of ore available at shallow depths in a number of underground mines in various parts of the world and increasing demand for metals induced by global economic growth, many underground mining activities are increasingly being carried out at greater depths. This obviously results in geomechanical environments that are more severe than those encountered at low depths. Thus, a direct consequence of these greater depths is the intensification of the aforementioned engineering geological hazards. In order to counteract or minimize the threats or hazards mentioned above in a cost-effective manner, the technology of cemented paste backfilling has been developed and widely applied in underground mines in the world (Ghirian and Fall 2013, 2014; Wang et al. 2016; Yilmaz 2018; Haruna and Fall 2020).

Cemented paste backfilling, a relatively newly developed mine backfilling method, has been widely adopted and used extensively by many mines worldwide (Brackebusch 1994; Hassani and Archibald 1998; Fall and Benzazoua 2003; Cui and Fall 2016a, b; Fang and Fall 2018). Cemented paste backfill (CPB) is made of tailings (soils or waste generated in a mine processing plant), water, and hydraulic binder. Chemical additives and/or synthetic fibers can be sometimes added to CPB to improve its engineering properties (e.g., Xue et al. 2019a, b). The main purpose of cemented paste backfilling technology is to guarantee the stability of the underground mining space or rock mass around excavations and, thus provide a safe working environment for mine workers. Moreover, this technology enables to eliminate or restrict many other mine induced geotechnical hazards, such as mine subsidence, rockbursts and roof-falls. Besides, the cemented paste backfilling technology is regarded as an environmental-friendly mining method for the underground disposal of tailings, which are a main source of acid mine drainage (AMD). In

addition to the safety and environmental benefits, cemented paste backfilling can also bring economic benefits to a mine. The support of a backfilling body underground allows complete exploitation of ore body and then improves the recovery ratio. The aforementioned advantages of cemented paste backfilling technology mainly explain its popularity in mining operations worldwide.

The underground CPB structure and its schematic diagram are depicted in Fig. 1, which shows that the priority of the geomechanical design of the CPB structure is to ensure its mechanical stability. Otherwise, the failure of CPB structures can result in financial ramifications and even fatalities. This mechanical stability is influenced by the shear characteristics or behaviour of the CPB–rock interface, as briefly discussed below. Moreover, shear properties of rock-mass/CPB interface play an important role in the transfer of stresses from the rock mass to CPB. The understanding and quantification of this stress transfer is crucial for the success of the geotechnical design of underground CPB structures, as discussed below.

In general, the bonded interface between dissimilar materials is often a weak link in terms of mechanical stability (Dong et al. 2017), and Nasir and Fall (2008) have concluded that both the adhesion and the friction angle of the CPB body are higher than those of the CPB–rock interface with a smooth surface. This means that, in cases of smooth rock interfaces (e.g., foliated rock) the shear failure can take place along the interfaces between the rock mass and CPB. Moreover, the occurrence of an arching effect, which is a result of shear stress redistribution and CPB consolidation, is also related to the interface shear performance or characteristics. The arching effect can transfer the CPB's vertical stress to the much stiffer surrounding rock via the interface, thereby decreasing the vertical stress within the CPB mass (Terzaghi 1943; Pirapakaran and Sivakugan 2007; Yang and Li 2015; Li and Fall 2016; Cao et al. 2019). Put differently, arching helps decrease the vertical stress in a CPB mass. Helinski et al. (2010) and Cui and Fall (2017) also observed this phenomenon experimentally and numerically, as shown in Fig. 2. The backfilling process in-situ is commonly divided into several steps, and the initial stress monitored by the bottom sensor increases with the filling operation, which is in good agreement with the development of self-weight stress (Fig. 2). However, after the initial backfilling

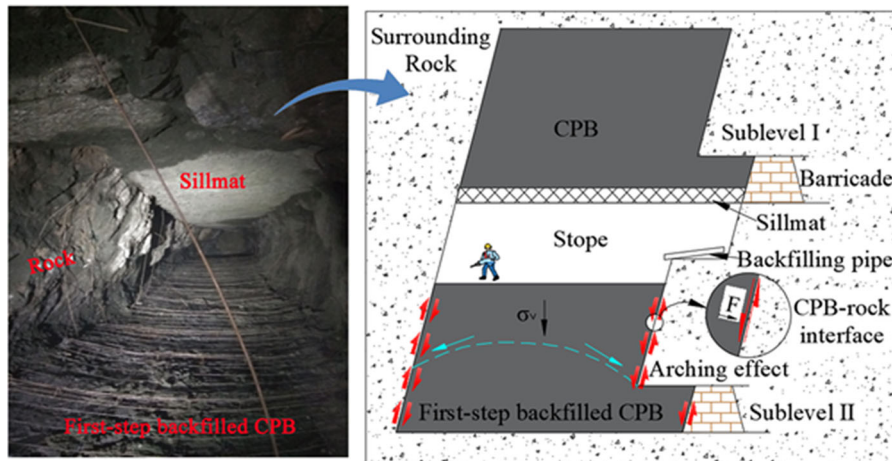


Fig. 1 Underground CPB structure and its schematic diagram

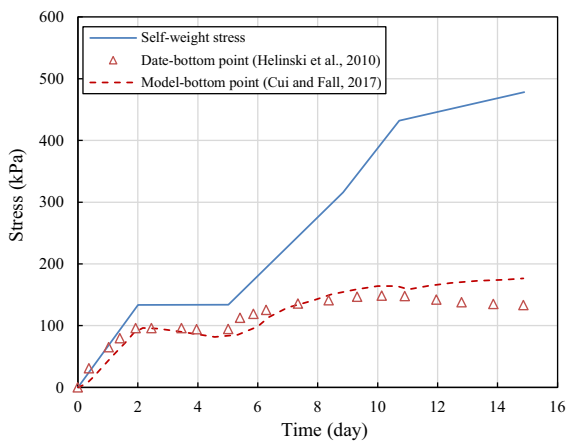


Fig. 2 Arching effects in CPB structure: Measured and predicted total stress versus time; self-weight stress versus time. Adapted from Cui and Fall (2017)

process (from the first day to the second day), the measured stress experiences a slight decrease (from the second day to the fifth day), and this reduction in stress is because of the stress redistribution, which means the occurrence of the arching effect. After the beginning of the second-step filling (fifth day), the measured stress at the bottom depicts a gradual increase, and the increasing rate is significantly lower than the expected increasing rate of self-weight stress. This means that the total stress induced by the overlying CPB body was mainly transferred to the surrounding rock through the arching effect. However, if arching is not present, the condition described in Fig. 2 would require a CPB body with a minimum

strength of 480 kPa to ensure its mechanical stability. This means a large amount of cement would be needed to achieve the required minimum strength, and consequently, the cost of the CPB would be significantly increased (Grice 2001; Yilmaz et al. 2003; Fall and Benzaazoua 2005; Kuganathan 2005; Orejarena and Fall 2011). The binder consumption can account for up to 75% of the backfill cost (Grice 2001; Fall et al. 2010). Therefore, the mechanical behaviour, especially the shear resistance capacity of the interface, is extremely important for a safer and more economical design of CPB structures.

A paucity of experimental studies have been conducted on the mechanical properties of the CPB–rock interface (e.g., Fall and Nasir 2010; Manaras et al. 2011; Koupouli et al. 2016; Fang and Fall 2018, 2019a, b). These studies have concluded that the shear behaviour of the interface is affected by several factors, such as normal stress, temperature, content of sulphate ions of the CPB material, and drainage condition. Despite the contributions of the aforementioned previous studies to understand the CPB–rock interface shear behaviour or properties better, a fundamental comprehension of the shear characteristics of the CPB–rock interface is still far from complete. Most of the previous studies on the CPB–rock interface consider only one type of rock, namely granite. However, given the different geological conditions of mines in different places, the type of rocks around the stope varies with each other. This means that the effect of different types of rocks on the shear behaviour or properties of CPB–rock is still

unknown or not well understood. Moreover, the effect of the rock surface roughness on the shear characteristics of the CPB–rock interface as well as the coupled effect of rock surface roughness and degree of cementation on the interface shear behaviour were ignored in the previous studies. In the field, the surface of the rock adjacent to or surrounding the CPB body can have various degrees of roughness. The surface of rock can also be characterized with various asperities, as shown in Fig. 1. Moreover, rock surface roughness has been acknowledged as one of the factors having a significant impact on the mechanical behaviour at the interface between rock and materials (e.g., soils, rock). Even though the interaction between geo-materials and rock with asperity surface has been extensively studied (Seidel and Haberfield 2002; Wang et al. 2015; Bahaaddini et al. 2015; He et al. 2017; Han et al. 2018), the knowledge of the shear performance of the interface between backfill structure and rough rock remains unknown. Moreover, the results of previous studies on the behaviour of the interface of rock with asperities and other geo-materials are not directly transferable to the CPB–rock interface because CPB is different from other geo-materials.

Considering the facts mentioned above, the major purpose of this research is to experimentally investigate the influence of rock surface roughness and CPB curing times as well as the rock type on the shear characteristics of CPB–rock interface, which is important for a thorough evaluation of the arching effect and geomechanical stability of CPB masses as well as for the safe and efficient design of CPB structures in the practice, as discussed previously. Therefore, it is of the practical engineering value to characterize this interface and elucidate its behaviour or evolution with respect to cementation and the aforementioned rock characteristics.

The present paper is organized as follows. Firstly, surface parameters used to evaluate surface roughness are introduced and discussed. Then, the experimental program conducted in this research is described. A large number of direct shear tests are conducted on interface samples with different interface roughness values. Subsequently, the obtained results are presented and discussed with respect to the influence of the rock type, rock surface roughness, combined effect of surface roughness and degree of cementation. Finally, the conclusions are presented.

2 Surface Parameters to Estimate Joint Roughness Coefficient

The difficulty in expressing the influence of the complex geometry of the asperity surface on the interface shear mechanical behaviour is addressed by introducing a simple coefficient, namely, joint roughness coefficient (JRC), which is initiated by Barton (1973) for evaluating the strength of rock joints with roughness:

$$\tau = \sigma \tan[JRC \log(JCS/\sigma) + \varphi_b] \quad (1)$$

where τ is the shear strength, σ is the applied normal stress, JCS is the compressive strength of the joint, and φ_b is the basic (residual) friction angle. Usually, according to Mohr–coulomb criterion, the whole part $[JRC \log(JCS/\sigma) + \varphi_b]$ is regarded as the friction angle. Herein, Barton specifically divided the friction angle into basic friction angle and the contribution of interface asperities. To determine the JRC of the targeted profile, ten surfaces with various JRC values (ranging from 0–20, where 0 means the smoothest and 20 refers to the roughest profile) were provided by

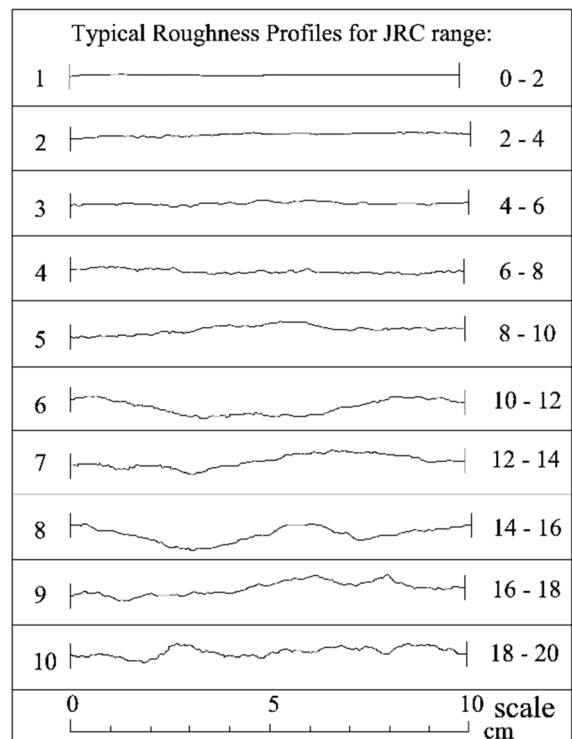


Fig. 3 Standard roughness profiles and their JRC values (Barton and Choubey 1977)

Barton and Choubey (1977), as shown in Fig. 3. The ISRM commission suggested that the JRC value of the targeted profile can then be determined by comparing it with the following standard surfaces (Brown 1981).

However, the determination of JRC value by visible comparison is inevitably considered as subjective. Hence, to evaluate the JRC value objectively and quantitatively, many surface parameters have been proposed. Tse and Cruden (1979) proposed several surface parameters, such as RMS (root mean square roughness index), CLA (arithmetical mean deviation roughness index), Z_2 (root mean square of the first deviation of the surface), MSV (mean square value roughness index), and SF (structure function of the profile) to estimate the JRC of a rock surface. But after analysing the correlation coefficient of eleven regression equations, they finally adopted Z_2 and SF to describe the JRC. However, Yu and Vayssade (1991) and Yang et al. (2001) found that the amplification of the surface would affect the evaluation of the JRC. Moreover, they also found the JRC is sensitive to the sampling interval. Therefore, they digitized ten standard profiles and adopted 200 discrete data points along the surface with different intervals, and finally improved the correlation coefficient of the regression equation. The ratio of the true length of profile to its projected length, R_p , was also proposed by EI-Soudani (1978) and related to JRC by Maerz et al. (1990). Another surface parameter, RL , which is similar to R_p , was developed by Yu and Vayssade (1991) to evaluate the JRC value. The aforementioned surface parameters and their relevant regression equations are summarized in Table 1.

Herein, the parameter Z_2 , is employed to evaluate the JRC value. To prepare CPB–rock interface

samples with different roughness values, some concrete bases with three different roughness measures, as shown in Fig. 4, are produced in this study. To accurately determine the JRC of concretes, a highly precise linear variable displacement transformer (LVDT) is used to survey the coordinates along the centerline at the concrete surface. The results of measured coordinates along the centerline are presented in Fig. 5. Thereafter, the following two estimation equations are adopted to calculate the JRC value (Yu and Vayssade 1991):

$$Z_2 = \left[\frac{1}{L} \sum \frac{(y_{i+1} - y_i)^2}{x_{i+1} - x_i} \right]^{1/2} \tag{2}$$

$$JRC = 32.69 + 32.98 \log Z_2 \tag{3}$$

where L is the nominal length of the digitized joint profile, and (x_i, y_i) are the coordinates of the discrete points. According to Eqs. (2) and (3), and the geometry of the prepared samples, the JRCs of the concrete surface prepared are calculated as 0, 6.5 and 16.6, respectively.

3 Experimental Program

3.1 Material Used

Synthetic tailings (silica tailings (ST)) were used as tailings materials. The ST are essentially made of quartz, which is the predominant mineral found in natural tailings from Canadian hard rock mines. Besides, given the pure component of ST (with 99.8% S_iO_2), the adoption of ST can then avoid

Table 1 Surface parameters and regression equations

Surface parameter	Calculation	Regression equation	Correlation coefficient	References
SF	$SF = \frac{1}{L} \sum (y_{i+1} - y_i)^2 \Delta x$	$JRC = 37.28 + 16.58 \log SF$	0.984	Tse and Cruden (1979)
Z_2	$Z_2 = \left[\frac{1}{L} \sum \frac{(y_{i+1} - y_i)^2}{x_{i+1} - x_i} \right]^{1/2}$	$JRC = 32.2 + 32.47 \log Z_2$ $JRC = 32.69 + 32.98 \log Z_2$	0.986 0.993	Tse and Cruden (1979) Yang et al. (2001)
R_p	$R_p = \frac{\sum_1^n \sqrt{(x_{i+1} - x_i)^2 + (y_{i+1} - y_i)^2}}{\sum_1^n (x_{i+1} - x_i)}$	$JRC = 558.68 \sqrt{R_p} - 557.13$	0.951	EI-Soudani (1978), Maerz et al. (1990)
RL	$RL = \frac{\sum_1^n \sqrt{(x_{i+1} - x_i)^2 + (y_{i+1} - y_i)^2}}{\sum_1^n (x_{i+1} - x_i)} - 1$	$JRC = 63.69 \sqrt{RL} - 2.31$	0.982	Yu and Vayssade (1991)

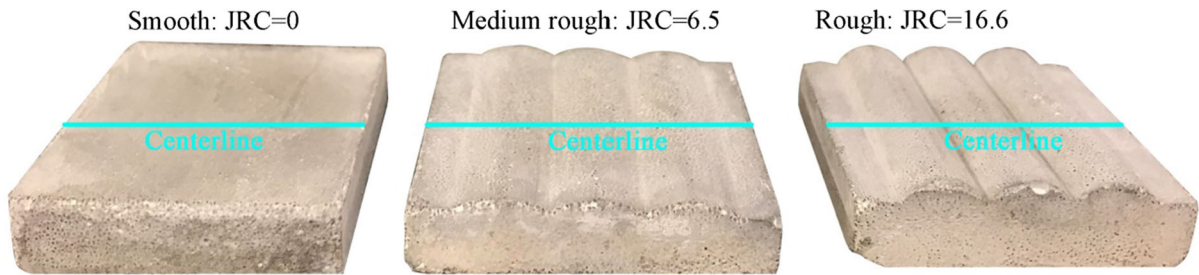


Fig. 4 Prepared concrete samples with three different JRC values (dimension of a sample: $60 \times 60 \times 15$ mm)

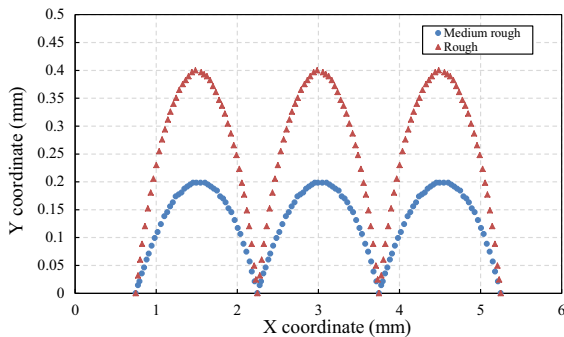


Fig. 5 Coordinates along the centerline

uncertainties in the results due to natural tailings, which can often interact with the cement hydration. Hence, the CPB part of the samples used in this paper are all produced by mixing ST, binder, and tap water. The Portland cement type I (PCI), a proportion of 4.5%, is used as the binder in this research. Meanwhile, the water-cement ratio is controlled as 7.35.

For the rock part of the samples, two kinds of rocks (e.g., marble and granite) and concrete are adopted. The use of concrete allows an easier preparation of rock surfaces with different roughness by using special plastic molds. The uniaxial compressive strength (UCS) of the marble ranges from 60 to 80 MPa, while that of granite (160 MPa) is much higher, which is noted in previous studies by the authors (Fang and Fall 2018, 2019a). In contrast, the concrete (with a strength of 38 MPa) is made of Portland cement type I (PCI), fine sand, and water with the weight ratio of 4:2:1.

3.2 Samples Preparation and Test Plans

3.2.1 Samples Preparation

The marble and granite are cut into small cuboid pieces with dimensions of $60 \times 60 \times 15$ mm; the

length and width are exactly the same as those of the direct shear box. To produce a concrete base with the same size, the mixed material (PCI: fine sand: water = 4:2:1) is cast into a plastic model (with three different levels of roughness) to form concrete. After being cured for 150 days (it is assumed that cement hydration is almost completed after 150 days), the concrete samples are then ready for producing CPB–concrete interface samples.

A B20F mixer is used to mix and stir the prepared materials (e.g., ST, PCI, and tap water), and to ensure the materials are fully mixed, the mixing process usually last 7 min. The slump of the prepared CPB is determined to be equal to 18 cm. The obtained paste is then poured into a plastic container (with an inner size of $60 \times 60 \times 30$ mm), in which the marble, granite or concrete has already been set. Thereafter, the air or oxygen in the CPB is squeezed out by manual vibration, and then the whole container is covered with a plastic film (to avoid evaporation). Some typical CPB–rock samples with different rock types and interface roughness are shown in Fig. 6.

3.2.2 Testing Plan

To determine the effects of rock types on the interface shear behaviour, the surface of the rocks (marble, granite, and concrete) are first polished smoothly, and then the interface samples are produced and cured for 1 day. Thereafter, three constant normal stresses, as shown in Table 2, are applied to the samples during the tests. Besides, to investigate the change in the shear characteristics of the CPB–rock interface with different roughness values and cementation degrees, the interface samples with JRC values of 0, 6.5 and 16.6 are also tested after being cured for 1, 7, and 28 days. To confirm the repeatability of the results, each test is

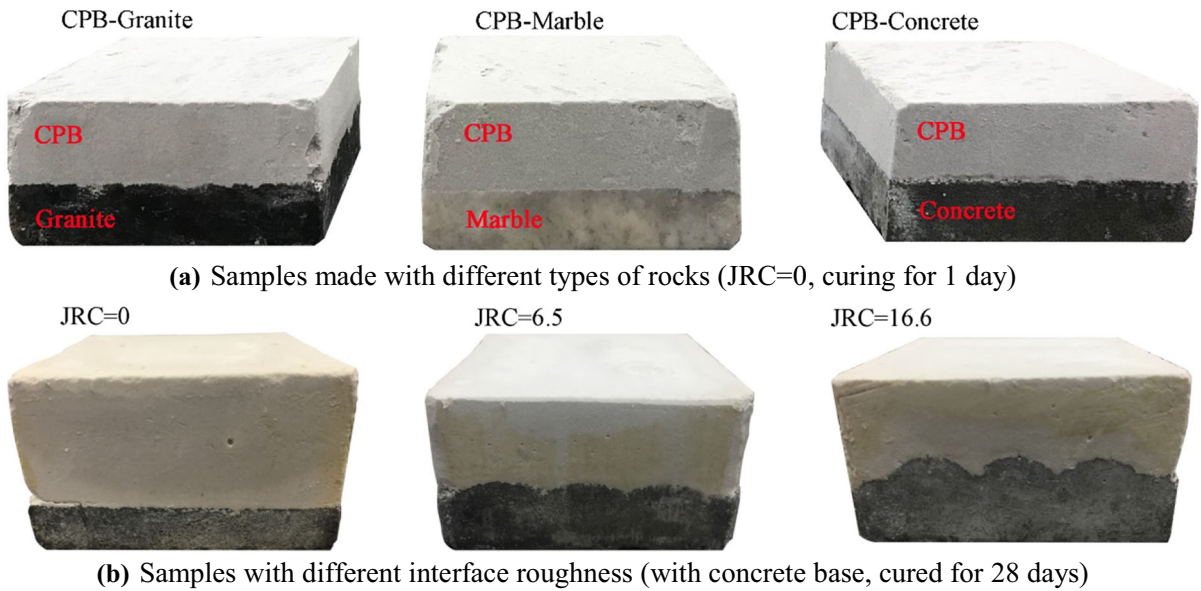


Fig. 6 Examples of prepared CPB–rock interface samples

Table 2 Experiment details

PCI content (%)	Water-cement ratio	Curing time (days)	Normal stress (kPa)	Rock type	Interface roughness
4.5	7.35	1	50	Marble, Granite, Concrete	0
4.5	7.35	1	100	Marble, Granite, Concrete	0
4.5	7.35	1	150	Marble, Granite, Concrete	0
4.5	7.35	1	50	Concrete	0, 6.5, 16.6
4.5	7.35	1	100	Concrete	0, 6.5, 16.6
4.5	7.35	1	150	Concrete	0, 6.5, 16.6
4.5	7.35	7	50	Concrete	0, 6.5, 16.6
4.5	7.35	7	100	Concrete	0, 6.5, 16.6
4.5	7.35	7	150	Concrete	0, 6.5, 16.6
4.5	7.35	28	50	Concrete	0, 6.5, 16.6
4.5	7.35	28	100	Concrete	0, 6.5, 16.6
4.5	7.35	28	150	Concrete	0, 6.5, 16.6

Slump of the CPB mixture ~ 18 cm

repeated 3 times. The experimental details are provided in Table 2.

3.2.3 Test Setup

A direct shear device is employed to conduct the direct shear tests according to ASTM D3080-04. Figure 7 shows the configuration of the direct shear device. It can be observed from the figure that a load cell is

installed and connected to the upper shear box to measure the shear force, while two LVDTs are adopted for displacement measurement. After the perpendicular application of the designed normal stress on the top of the samples, the lower shear box moves horizontally with a rate of 0.5 mm per minute. During the test, the upper shear box is maintained stationary. A computer software, Labview, is used to record the data of the tests.

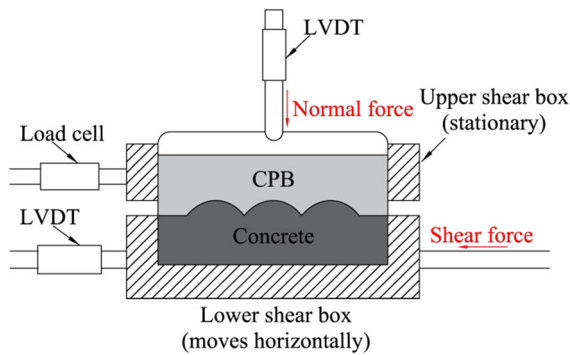


Fig. 7 Configuration of direct shear test device

3.3 Microstructural Analyses

Two main microstructural analyses, including thermal analysis and scanning electron microscope (SEM), are used here to investigate the progress of the cement hydration as well as the microstructure of the interface, respectively. The thermal analysis is carried out on cement paste of CPB (with $w/c = 1$ to simulate the high water content of CPB) with a Q5000IR thermogravimetric analyzer, which can record the weight loss of cement paste with the temperature increasing to 1000 °C. In contrast, the SEM observation is performed on intact interface samples with a Hitachi 3500-N microscope, which allows the analysis of the texture and the pore structure at the interface microscopically. Prior to the abovementioned two tests, samples are all subjected to a drying process (at a temperature of 45 °C for 4 days) to stop the cement hydration. Stopping the cement hydration in cementitious materials is needed to prepare samples for many techniques of microstructural analysis.

4 Results and Discussions

Typical results of the direct shear tests are presented and discussed in this section. The effect of the rock type on the interface shear performance is briefly introduced in Sect. 4.1, while the influences of roughness and cementation are addressed in Sect. 4.2, respectively.

4.1 Influence of the Type of Rock on Interface Shear Performance

Figure 8 presents the shear behaviour of the interface samples with different rock bases of granite, marble, and concrete (cured for 1 day). The results show that the shear curves of all samples show a similar tendency, and rock type has limited effects on both shear strength and dilation. The shear displacement-shear stress curve first depicts an increase up to peak shear stress (strain hardening behaviour), followed by a slight decrease (strain softening behaviour). Besides, the shear strength varies from 70 to 82 kPa for samples with different type rocks (with a normal stress of 100 kPa). In terms of the normal displacement of interface samples, all samples (conducted under normal stresses of 50 kPa and 100 kPa) first experience an initial contraction, as can be seen from the figures in the right column of Fig. 8. This initial contraction is attributed to the inherent compressibility of CPB, and the compressibility of the early-age samples decreases with time (Fang and Fall 2018). The study conducted by Nasir and Fall (2008) also indicated the same contraction behaviour. Thereafter, it shows a slight dilation until the shear stress reaches its peak value (shear strength). The magnitude of shear dilation is associated with the degree of cement hydration, whose mechanism is introduced in detail below. For subsequent shear displacement beyond the point with the highest shear dilation, the shear displacement-normal displacement curve is then characterized by continuous contracting behaviour. In contrast, the high normal stress (150 kPa) restricts the normal displacement at the interface, and as a result, the shear displacement-normal displacement curves all depict contraction behaviours, regardless of the type of rock.

The evolution of shear strength with normal stresses of the corresponding interface samples is shown in Fig. 9, based on which, the shear envelopes can be easily obtained by linear regression fitting. The Mohr–Coulomb criterion is used to establish the shear failure envelope of the CPB–rock interface since the R^2 values of the fitted regression lines are almost equal to 1. Hence, the shear strength parameters of the interface are easily derived, which are also indicated in the figure. The results show that the difference in the mechanical properties (e.g., shear strength, friction angle) of the interface samples made with different

Fig. 8 Evolution of shear stresses and normal displacements of interface samples produced with different rock types: **a** Granite, **b** Marble **c** Concrete (with a curing time of 1 day)

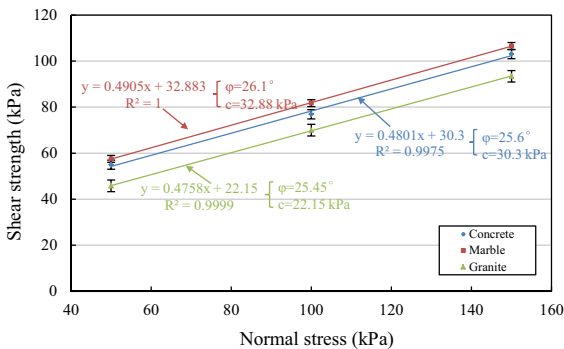
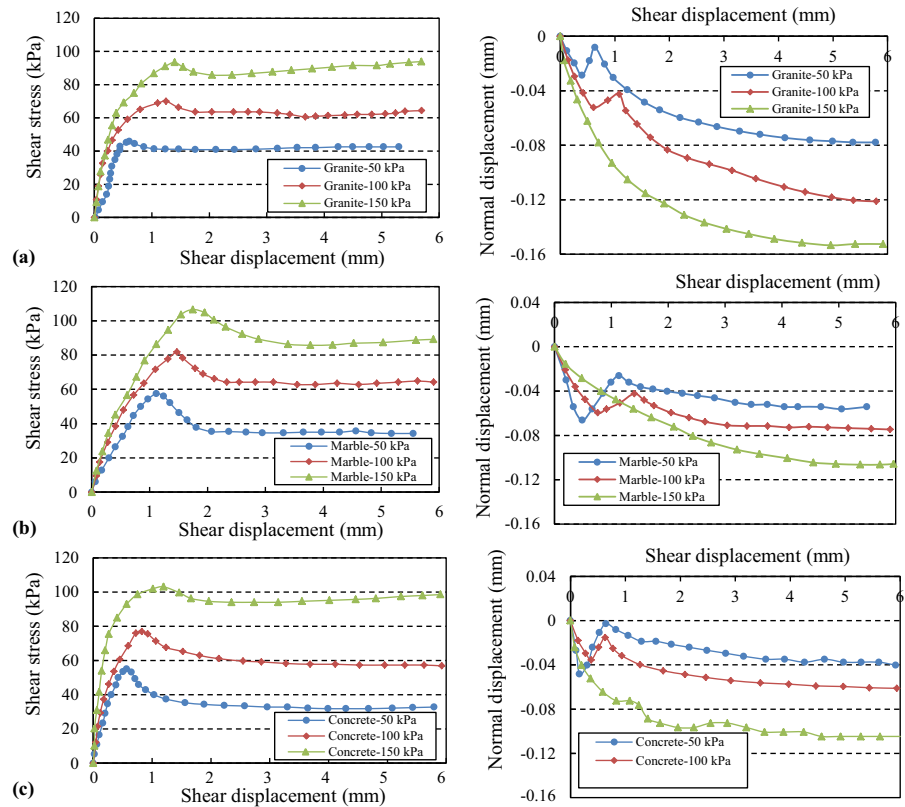


Fig. 9 Shear envelopes of the interface between CPB and different type of rocks (cured for 1 day)

rocks is insignificant, especially the friction angle. This observation means that the type of rocks considered in this study has limited influence on the shear properties of the interface. This minor or insignificant of the rock type on the interface shear characteristics is related to the fact that the failure occurs in the interface and the interfacial transition zone, as discussed below.

The failure of the interface between CPB and different types of rock is because of the existence of

the interfacial transition zone (ITZ), which is also observed in many studies on other geotechnical structures involving cementitious material (Breton et al. 1993; Ke et al. 2010). The ITZ is characterized by high porosity. This phenomenon is also known as the “wall” effect (Diamond and Huang 2001; Scrivener et al. 2004). The formation of the ITZ is due to the penetration of cement paste into the pore structure; this ITZ then bonds CPB and rock together. The result of SEM analyses, as presented in Fig. 10, attests to this argument. The interface crack is clearly observed, which is marked by a red dashed line in the figure. Besides, between the interface and granite, a thin layer of ITZ is also observed. This result of SEM analyses also agrees with the interface model proposed by He et al. (2017) on the interface between new and old concrete. Moreover, the results of SEM analysis ($\times 1500$, presented in the right of Fig. 10) on granite, marble, and mature concrete show a similar observation, which are all characterized by a denser structure. This reconfirms the limited effects of rock type (considered in this research) on the interface shear performance. It should be emphasized that a rock with

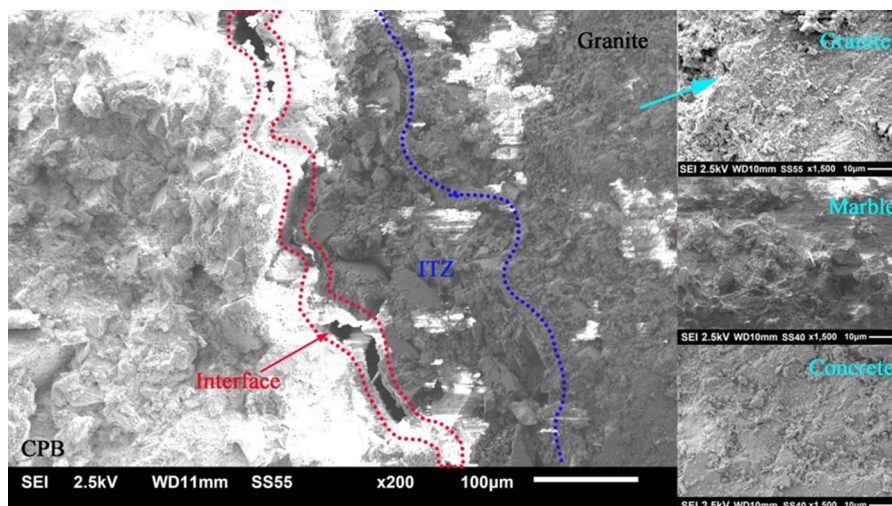


Fig.10 SEM images of the interface

a strength lower than that of the CPB could result in a different interface shear behavior.

4.2 Influence of Roughness and Cementation on the Interface Shear Behaviour

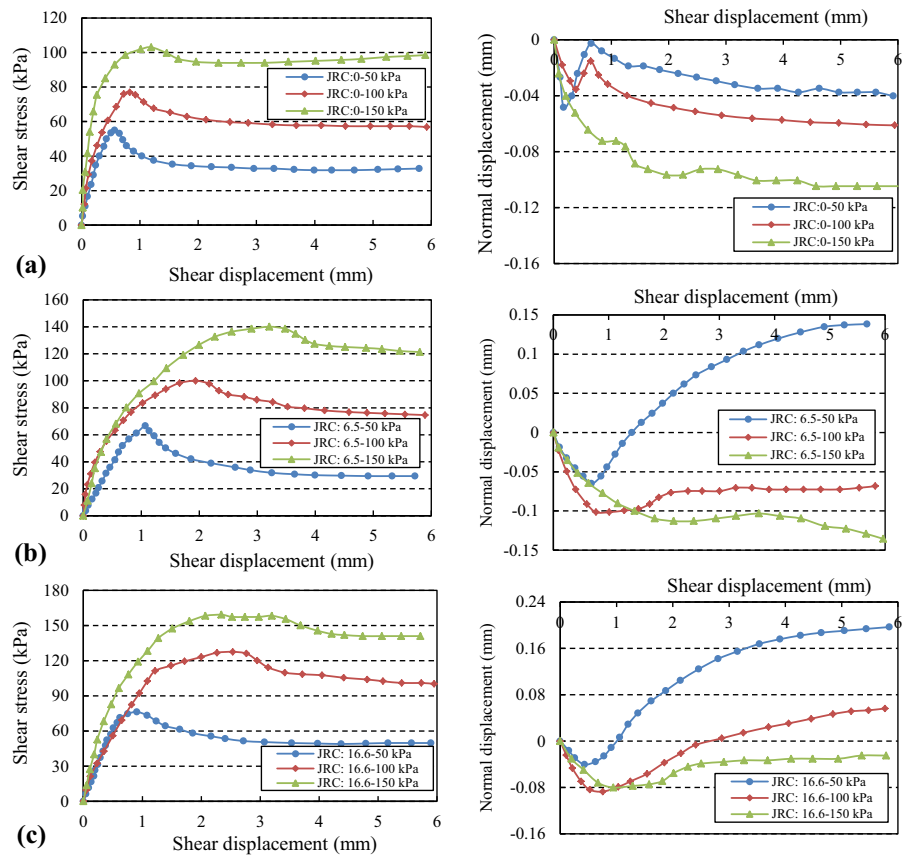
4.2.1 Influence of Interface Roughness

The shear characteristics of the CPB–concrete samples with three various roughness measures (e.g., JRC = 0, 6.5, 16.6) are shown in Fig. 11. Obviously, from the figure, it can be observed that the shear strength of the interface samples is considerably affected by the interface roughness. Specially, the peak shear stress rises with the increasing roughness, and this observation is in agreement with the conclusions made by Chen et al. (2015) and Fang and Fall (2019a). For instance, for samples conducted under 50 kPa normal stress, the shear strength of smooth interface sample is 55 kPa, while those of samples with roughness of JRC = 6.5 and JRC = 16.6 are 67 kPa and 76 kPa, respectively. The slight rise in shear strength with rougher interfaces is because of the increasing size of the asperity at the interface. In other words, the interlocking structure becomes larger as the roughness of the concrete surface increases. This argument is macroscopically attested to by the interface pictures taken after the direct shear test, as shown in Fig. 14. The size of the interlocking structure of the rough interface sample (JRC = 16.6) is larger than that of the medium rough interface (JRC = 6.5), as

indicated in Fig. 14, for example, $L2 > L1$. However, the shear strength of the sample with a JRC of 6.5 is 21.3% higher than that obtained from the tests performed with a smooth interface (conducted with 50 kPa normal stress). In contrast, for the test with an even rougher surface (JRC = 16.6), the increase in the peak shear stress with respect to the sample with a JRC of 6.5 is less than 14.4%. In other words, the increased stress is not proportional to the difference in roughness, and the difference in shear strength for the medium rough surface with respect to the smooth surface is higher than that between the medium rough and the roughest surface. This phenomenon is also observed by the study on the sand–steel interface conducted by Han et al. (2018). The significant difference in shear strength (comparison between smooth and medium rough interface samples) indicates the strength of the interlocking structure contributes a lot to the shear strength of the interface. In contrast, the comparatively smaller difference in shear strength between the medium rough and the rough interface means the size of the interlocking structure has a less significant influence on the evolution of the shear strength.

Similar to the normal displacement of the smooth interface introduced in Sect. 4.1, the interface samples with roughness also experience contraction due to the inherent compressibility of CPB at first. Thereafter, most interface samples experience obvious dilation (with the exception of samples conducted with 150 kPa normal stress), and the magnitude of the

Fig. 11 Evolution of shear stresses and normal displacements with shear displacements at curing time of 1 day: **a** JRC = 0, **b** JRC = 6.5 **c** JRC = 16.6



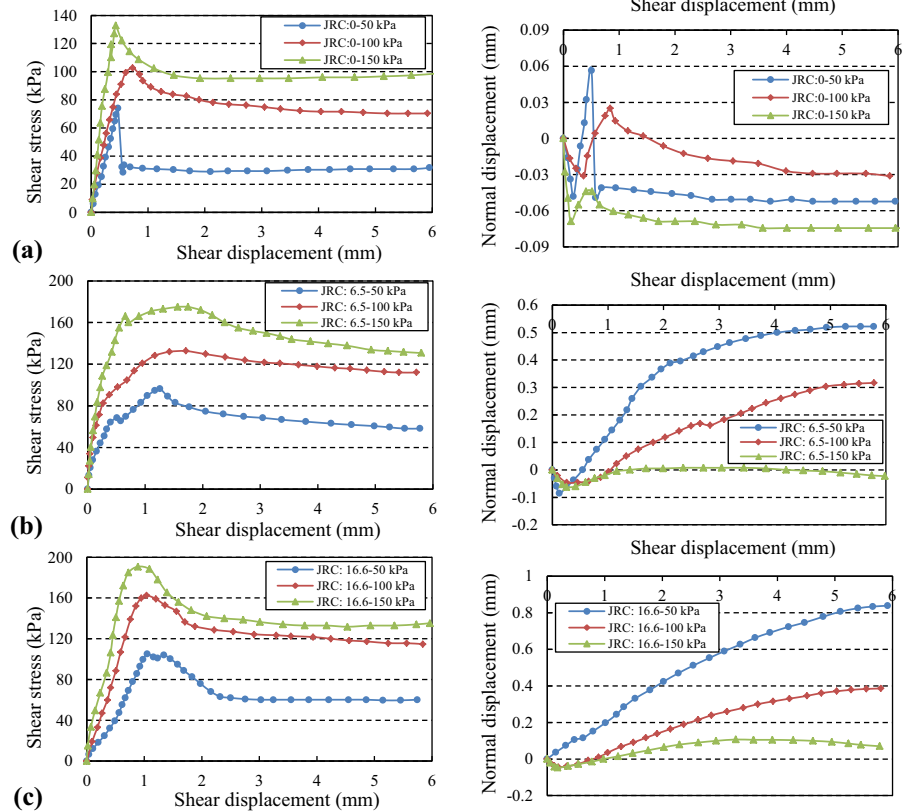
shear dilation is closely related to the interface roughness. Take the samples conducted with 50 kPa normal stress as examples, the shear dilation of the interface samples with JRC = 0, 6.5, and 16.6 are 0.05 mm, 0.2 mm and 0.24 mm, respectively. In addition, the magnitude of shear dilation of interface samples decreases significantly with normal stress, and this reduction in the amount of shear dilation is owing to the suppression of normal stress on relative separation at the interface. In other words, before the further increase in normal displacement, the major asperities at the interface cannot sustain the increasing normal stress, and then failure occurs. The continuous contraction-less pronounced shear dilation of interface samples subjected to 150 kPa normal stress is also attributed to this mechanism. Another interesting phenomenon is that the smooth interface samples suffer from contracting behaviour for subsequent shear displacement beyond the point with the highest shear dilation, whereas the interfaces with rougher surface experience a continuous increase in shear

dilation, and this is especially obvious for samples sheared at lower normal stresses (e.g., 50 kPa).

4.2.2 Coupled Effect of cementation and Surface Roughness

Figures 11, 12 and 13 show the effects of cementation on the shear performance of CPB–concrete samples with different interface roughness values (Fig. 14), and Fig. 15 presents the evolution of peak shear stress with time. It is observed from the figures that both peak shear stress and normal displacement are influenced by the curing time and interface roughness. For example, the CPB–concrete interface cured for 28 days has the highest shear strength, followed by samples cured for 7 days, and 1 day, regardless of interface roughness. Besides, the shear stiffness of the interface sample also increases with curing time. These time-dependent changes are consistent with conclusions drawn by other researchers (Nasir and Fall 2008; Koupouli et al. 2016). Actually, the curing time-

Fig. 12 Evolution of shear strength and normal displacements with shear displacements at curing time of 7 days: **a** JRC = 0, **b** JRC = 6.5, **c** JRC = 16.6

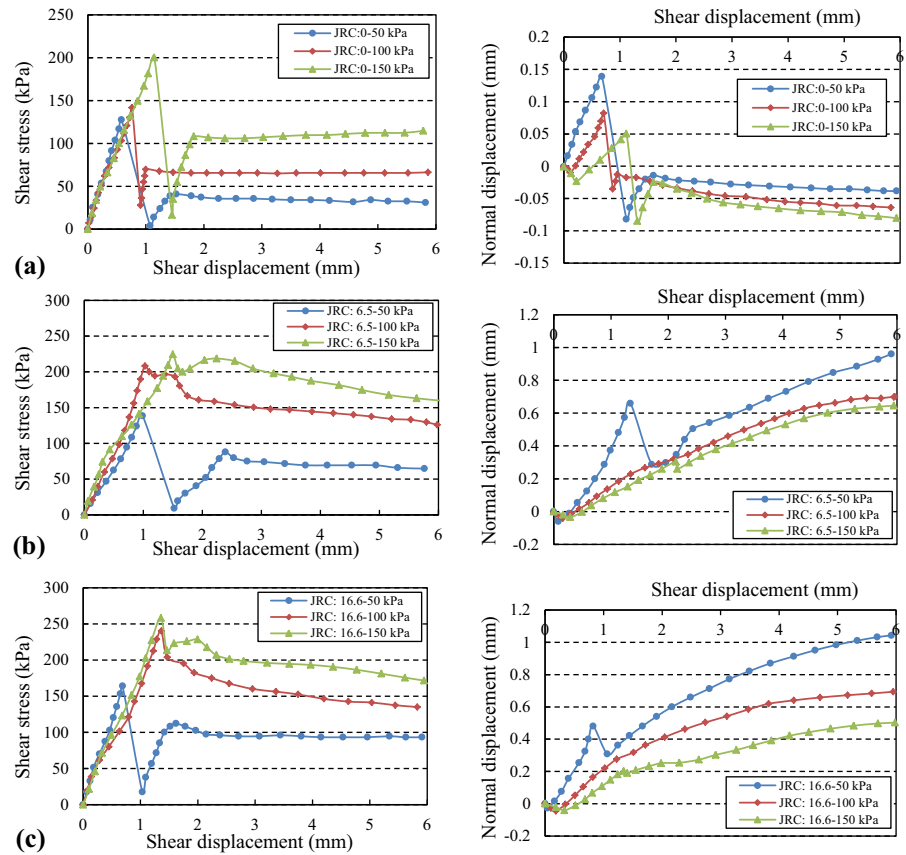


induced increases in shear strength and shear stiffness are due to the progress of cement hydration in CPB. It is known that calcium silicate hydrate (C–S–H), a bonding phase in cementitious materials, is a major product of cement hydration, the degree of which raises with curing time (Taylor 1964; Gani 1997; Pokharel and Fall 2013). As a result, the quantity of C–S–H also increases with time, thereby leading to high shear strength at the CPB–concrete interface. The rising amounts of C–S–H with time are supported by the results of thermal analysis on cement paste cured for 7 days and 28 days, as shown in Fig. 16. The weight change at a temperature of 30–200 °C in the figure is owing to the dehydration of C–S–H and gypsum (Sha et al. 1999; Jiang et al. 2016, 2017), while the weight loss range from 400 to 450 °C is due to the disintegration of calcium hydroxide (Nonnet et al. 1999; Zhou and Glasser 2001). The higher weight loss of the 28 day sample at a temperature from 30 to 200 °C (in comparison to the date of the 7 day sample) means larger amounts of C–S–H are generated in the long-cured sample. In addition to the shear

strength, it can also be noted from Figs. 11, 12 and 13 that the magnitude of initial contraction decreases with curing time, while the shear dilation increases with curing time. This observed reduction in initial contraction and increase in shear dilation is also because of the raised degree of cement hydration. Specifically, the cement hydration process consumes large amounts of water, and this then decreases the water content in the CPB; as a result, the effective stress is increased. On the other hand, the precipitation of expansive minerals (e.g., gypsum, ettringite) with time refines the capillary pore, which decreases the compressibility. The larger shear dilation with time is owing to the development in both size and strength of asperity.

The results presented in Figs. 11, 12 and 13 also show that the interface samples with roughness, especially those sheared at high normal stress, tend to experience two peak shear stresses during the shear test. This is very obvious for long-cured samples, as shown in Fig. 13b. The first peak stress—which is in the same vein as the stress peak that occurred in the smooth interface—is because of the loss of the binding

Fig. 13 Evolution of shear strength and normal displacements with shear displacements at curing time of 28 days: **a** JRC = 0, **b** JRC = 6.5 **c** JRC = 16.6



force between CPB and concrete. To some degree, this effect is similar to the wall effect of the cement grains against the aggregate, and this phenomenon is regarded as the loss of adhesion. Saiang et al. (2005) also observed the same phenomenon in their study on the interface between concrete and rock. The second peak in shear stress is attributed to the failure of the interlocking structure. Specifically, as a consequence of the relative motion of the asperity at the non-cemented CPB–concrete interface, the shear dilation is increased. Besides, the contacting area between CPB and concrete is decreased. Consequently, the normal stress keeps increasing with shear dilation until reaching the strength of the major asperity at the interface. Thereafter, the failure of the interlocking structure corresponds to the second peak stress.

It can also be observed from Figs. 11, 12 and 13 that the shear dilation increases with curing time, regardless of interface roughness. For the smooth CPB–concrete interface conducted with 50 kPa normal stress, the shear dilation increases from 0.05 mm on

the first day to 0.14 mm on the twenty-eighth day. In contrast, the shear dilation of the roughest interface samples (JRC = 16.6) rises from 0.24 mm to 1.07 mm during the same curing period. The increased shear dilation of the CPB–concrete interface with time is due to (1) the refined pore structure of CPB, and (2) the stronger interlocking structure, as results of the raised degree of cement hydration, which was discussed previously.

4.3 Evolution of Mechanical Properties of CPB–Concrete Interface with Different Roughness

Given the significant effects of interface roughness on the evolution of the mechanical strength of rock joints, Barton (1973) took the roughness into consideration and proposed Eq. (1) to estimate the shear strength of rough rock joints. However, Manaras et al. (2011) found the shear strength derived from Barton’s equation is lower compared to measured samples. Considering the significant role of adhesion in

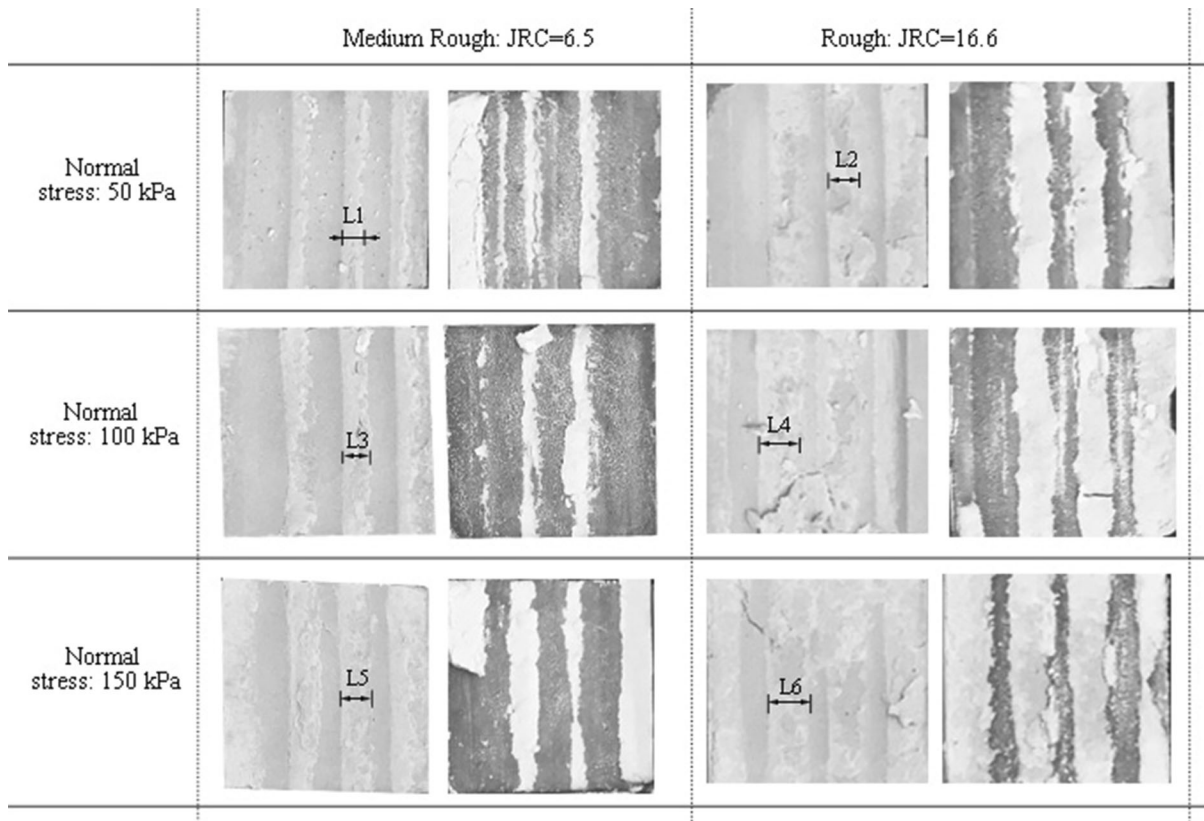


Fig. 14 Pictures of interface of samples after direct shear test (cured for 7 days)

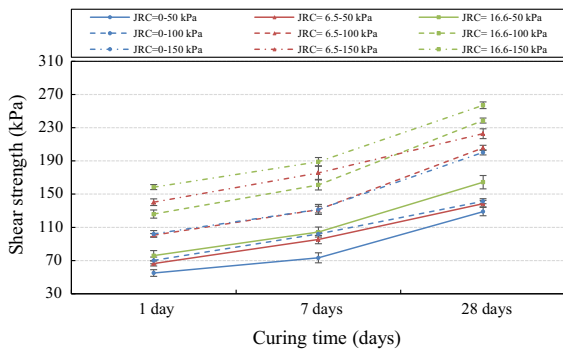


Fig. 15 Evolution of peak shear stress of CPB–concrete interface with time

predicting the shear strength of cementitious materials, a revised version of Barton’s equation is adopted here to deduce the shear properties of the CPB–concrete interface:

$$\tau = \sigma \tan[JRC \log(JCS/\sigma) + \varphi_b] + c \tag{4}$$

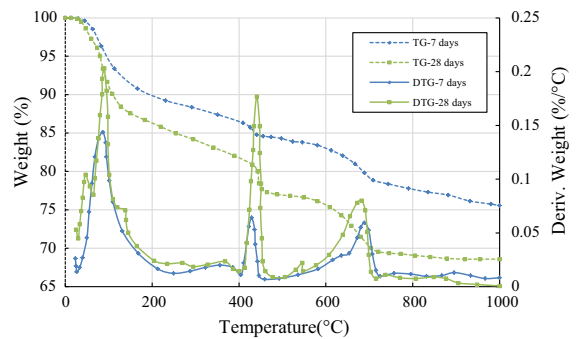


Fig. 16 Results of TG and DTG analyses on CPB (cured for 7 and 28 days)

where c is the adhesion of the interface. The JCS value here is the UCS of the CPB, which is also associated with the degree of binder hydration. According to the tests conducted by Fall et al. (2010), the UCS of standard CPB samples cured for 1 day, 7 days, and 28 days are 150 kPa, 444 kPa and 624 kPa, respectively. Therefore, based on the data on the shear

strength-normal stress at the interface, the shear strength envelopes of the interface samples can be obtained, and then the mechanical parameters of the interface (e.g., friction angle, adhesion) can be deduced.

Figure 17 presents the evolution of shear parameters (e.g., friction angle, adhesion) of the studied rough interface. The figure shows that these properties are significantly affected by time. Specifically, the adhesion of the interface increases with curing time, as a result of the increasing degree of binder hydration (Nasir and Fall 2008; Fang and Fall 2018). Besides, the rougher interface tends to experience higher adhesion, regardless of curing time. The roughness-induced increase in adhesion is due to the increased contact area between CPB and concrete. In contrast, the evolution of the friction angle is complex. For the smooth interface (JRC = 0), the friction angle rises with curing time, which coincides with the conclusion made by Nasir and Fall (2008) and Fang and Fall (2019a). However, for the interface sample with roughness, the evolution of the friction angle varies with the failure criterion adopted. In other words, if the Mohr–coulomb failure criterion is used, the friction angle presents an increasing tendency with time, the value of which is shown in Table 3. However, the effective friction angle depicts a decreasing tendency in the first 7 days by adopting a revised Barton’s equation, as shown in Fig. 17. In other words, the roughness contributes a lot to the development of the friction angle, and after extracting the contribution caused by roughness, the effective friction angle decreases with time.

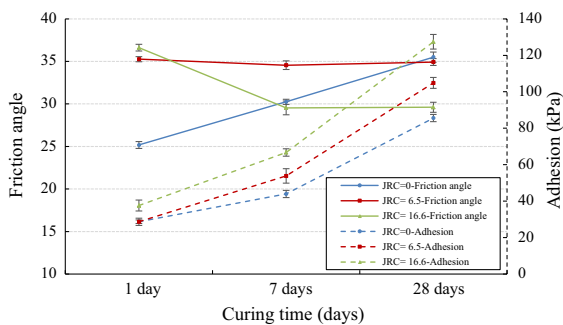


Fig. 17 Evolution of the adhesion and effective friction angle of the CPB–concrete interface

Table 3 Evolution of friction angle (according to Mohr–Coulomb criterion)

Interface roughness	Friction angle		
	1 day	7 days	28 days
Smooth (JRC = 0)	25.2	30.3	35.5
Medium rough (JRC = 6.5)	36.4	38.8	40.1
Rough (JRC = 16.6)	39.5	40.3	42.8

5 Summary and Conclusions

The paper presents new experimental results of direct shear tests on the interface between CPB and surrounding rock (with different roughness values). An extensive program of direct shear tests and microstructural analysis has been conducted to gain insights into the effect of different types of rock, rock surface roughness and degree of cementation as well as the coupled effects of these factors on the shear properties and behaviour of the interface between cemented paste backfill (CPB) and rock. The following conclusions are made:

- Three kinds of rocks or materials (e.g., granite, marble, and concrete) are used as the rock part of the interface samples. The results of direct shear tests on 1 day interface samples show that all samples experience similar shear behaviour, regardless of the type of rock used. Besides, the effect of the type of rock on the friction angle and the shear strength of the interface are also limited. The type of rock considered in this study has limited effects on both shear strength and dilation too. However, it should be underlined that a rock weaker than the rocks considered in this study or CPB could show a different behavior. This issue should be addressed in the future.
- Surface parameter, Z_2 , is adopted to estimate the surface roughness in this study, and three kinds of concrete with different roughness values (e.g., JRC = 0, JRC = 6.5 and JRC = 16.6) are produced to investigate the contribution of roughness to the interface shear strength. The obtained results have shown that the shear strength of the rough interface increases with roughness. This increase in shear strength is due to the larger interlocking structure with more roughness. However, the

increased stress is not proportional to the difference in roughness. It is also found that the interface samples with roughness, especially those sheared at high normal stress, tend to experience two peak shear stresses during the shear test.

- The results of the SEM analysis of the CPB–rock interface have indicated that the failure of the interface is due to the existence of the interfacial transition zone (ITZ). This ITZ is characterized by high porosity.
- The peak shear stress and shear dilation of the interface samples increase with curing time, as a result of the raised degree of binder hydration. The specific mechanisms are (1) a large amount of moisture was consumed by binder hydration; (2) some expansive products (e.g., ettringite) of cement hydration refine the pore structure at the interface; (3) the increasing amount of C–S–H enhances the binding force at the interface, thereby increasing the strength of the interlocking structure. However, curing times up to 28 days were considered in this study. Longer curing times (90–180 days) should be investigated in the future.
- The adhesion of the interface samples increases with both curing time and roughness. The curing time-induced increase in adhesion is due to the increased degree of cement hydration with time, while the roughness-induced increase is because of the larger contact area between CPB and concrete. Meanwhile, the friction angle of the smooth interface also depicts a rising tendency with time. However, with respect to the interface with roughness, the effective friction angle decreases with time.

Despite the results and findings presented in this manuscript, the scale effect on the rock–backfill interface shear behaviour was not considered in this study. This will be the object of future investigations. Moreover, it will be interested to investigate the shear behaviour of the interface between CPB and weak rocks in the future.

Acknowledgements The University of Ottawa, the Natural Sciences and Engineering Research Council of Canada (NSERC), and the China Scholarship Council (CSC) are acknowledged by the authors for their support. Also, the authors want to thank Mr. Glenn for his help on the SEM analysis.

References

- Bahaaddini M, Hagan PC, Mitra R, Hebblewhite BK (2015) Parametric study of smooth joint parameters on the shear behaviour of rock joints. *Rock Mech Rock Eng* 48:923–940
- Barton N (1973) Review of a new shear strength criterion for rock joints. *Eng Geol* 7(4):287–332
- Barton N, Choubey V (1977) The shear strength of rock joints in theory and practice. *Rock mechanics* 10(1):1–54
- Brackebusch FW (1994) Basics of paste backfill systems. *Min Eng* 46:1175–1178
- Breton D, Carles-Gibergues A, Ballivy G, Grandet J (1993) Contribution to the formation mechanism of the transition zone between rock–cement paste. *Cem Concr Res* 23(2):335–346
- Brown ET (1981) *Rock characterization testing and monitoring (ISRM suggested methods)*. Pergamon, Oxford
- Cao S, Yilmaz E, Xue G, Song W (2019) Assessment of acoustic emission and triaxial mechanical properties of rock-cemented tailings matrix composites. *Adv Mater Sci Engg*. Article 6742392:12p. <https://doi.org/10.1155/2019/6742392>
- Chen X, Zhang J, Xiao Y, Li J (2015) Effect of roughness on shear behaviour of red clay–concrete interface in large-scale direct shear tests. *Can Geotech J* 52:1122–1135
- Cui L, Fall M (2016a) An evolutive elasto-plastic model for cemented paste backfill. *Comput Geotech* 71:19–29
- Cui L, Fall M (2016b) Mechanical and thermal properties of cemented tailings materials at early ages: influence of initial temperature, curing stress and drainage conditions. *Constr Build Mater* 125:553–563
- Cui L, Fall M (2017) Multiphysics modeling of arching effects in fill mass. *Comput Geotech* 83:114–131
- Diamond S, Huang J (2001) The ITZ in concrete—a different view based on image analysis and SEM observations. *Cem Concr Compos* 23(2–3):179–188
- Dong W, Yang D, Zhou X, Kastiukas G, Zhang B (2017) Experimental and numerical investigations on fracture process zone of rock–concrete interface. *Fatigue Fract Eng M* 40(5):820–835
- El-Soudani SM (1978) Profilometric analysis of fractures. *Metallogr* 11:247–336
- Fall M, Benzaazoua M (2003) Advances in predicting performance properties and cost of paste backfill. *Int. Conf. Tailings Mine Waste, Colorado, USA*, pp 12–15
- Fall M, Benzaazoua M (2005) Modeling the effect of sulphate on strength development of paste backfill and binder mixture optimization. *Cem Concr Res* 35(2):301–314
- Fall M, Nasir O (2010) Mechanical behaviour of the interface between cemented tailings backfill and retaining structures under shear loads. *Geotech Geo Eng* 28:779–790
- Fall M, Célestin JC, Han FS (2009) Suitability of bentonite–paste tailings mixtures as engineering barrier material for mine waste containment facilities. *Miner Eng* 22(9–10):840–848
- Fall M, Célestin JC, Pokharel M, Touré M (2010) A contribution to understanding the effects of temperature on the mechanical properties of cemented mine backfill. *Eng Geol* 14(3–4):397–413

- Fang K, Fall M (2018) Effects of curing temperature on the shear behaviour of cemented paste backfill–rock interface. *Int J Rock Mech Min* 112:184–192
- Fang K, Fall M (2019a) Chemically induced changes in the shear behaviour of the interface between rock and tailings backfill undergoing cementation. *Rock Mech Rock Eng* 52:3047–3062
- Fang K, Fall M (2019b) Effect of curing stress, drainage condition and filling rate on shear behaviour of the interface between cemented paste backfill and rock. *Rock Mech Rock Eng* 53:325–336
- Gani MSJ (1997) *Cement and concrete*. Chapman & Hall, London
- Ghirian A, Fall M (2013) Coupled thermo-hydro-mechanical-chemical behaviour of cemented paste backfill in column experiments. Part I: physical, hydraulic and thermal processes and characteristics. *Eng Geol* 164:195–207
- Ghirian A, Fall M (2014) Coupled thermo-hydro-mechanical-chemical behaviour of cemented paste backfill in column experiments. Part II: mechanical, chemical and microstructural processes and characteristics. *Eng Geol* 170:11–23
- Grice T (2001) Recent mine developments in Australia. Proceedings of the 7th international symposium on mining with backfill (MINEFILL), p 351–357
- Haruna S, Fall M (2020) Time-and temperature-dependent rheological properties of cemented paste backfill that contains superplasticizer. *Powder Technol* 360:731–740
- Han F, Ganju E, Salgado R, Prezzi M (2018) Effects of interface roughness, particle geometry, and gradation on the sand–steel interface friction angle. *J Geotech Geoenviron* 144(12):04018096
- Hassani F, Archibald J (1998) *Mine backfill*. Canadian Institute of Mine, Metallurgy and Petroleum, Canada
- He Y, Zhang X, Hooton R, Zhang X (2017) Effects of interface roughness and interface adhesion on new-to-old concrete bonding. *Constr Build Mater* 151:582–590
- Helinski M, Fahey M, Fourie A (2010) Behavior of cemented paste backfill in two mine stopes: measurements and modeling. *J Geotech Geoenviron* 137(2):171–182
- Jiang HQ, Fall M, Cui L (2016) Yield stress of cemented paste backfill in sub-zero environments: experimental results. *Miner Eng* 92:141–150
- Jiang H, Fall M, Cui L (2017) Freezing behaviour of cemented paste backfill material in column experiments. *Construct Build Mater* 147:837–846
- Ke Y, Ortolá S, Beaucour A, Dumontet H (2010) Identification of microstructural characteristics in lightweight aggregate concretes by micromechanical modelling including the interfacial transition zone (ITZ). *Cem Concr Res* 40(11):1590–1600
- Koupouli NJF, Belem T, Rivard P, Effenguet H (2016) Direct shear tests on cemented paste backfill–rock wall and cemented paste backfill–backfill interfaces. *J Rock Mech Geotech Eng* 8(4):472–479
- Kuganathan K (2005) Geomechanics of mine fill. In: Potvin Y, Thomas E, Fourie A (eds) *Handbook on mine fill*. Australian centre of Geomechanics, Australia, pp 23–49
- Li W, Fall M (2016) Sulphate effect on the early age strength and self-desiccation of cemented paste backfill. *Constr Build Mater* 106:296–304
- Maerz NH, Franklin JA, Bennett CP (1990) Joint roughness measurement using shadow profilometry. *Int J Rock Mech Min Sci Geomech Abstr* 27(5):329–343
- Manaras E, De-Souza, Archibald JF (2011). Strength behaviour and failure mechanisms of backfill–rock mass interfaces. Paper presented at the 10th international conference on mining with backfill, The southern African Institute of Mining and Metallurgy, Cape Town, South Africa, 2011
- Nasir O, Fall M (2008) Shear behaviour of cemented pastefill–rock interfaces. *Eng Geol* 101(3):146–153
- Nonnet E, Lequeux N, Boch P (1999) Elastic properties of high alumina cement castables from room temperature to 1600 °C. *J Eur Ceram Soc* 19(8):1575–1583
- Orejarena L, Fall M (2011) Artificial neural network based modeling of the coupled effect of sulphate and temperature on the strength of cemented paste backfill. *Can J of Civil Eng* 38(1):100–109
- Pirapakaran K, Sivakugan N (2007) Arching within hydraulic fill stopes. *Geotech Geol Eng* 25:25–35
- Pokharel M, Fall M (2013) Combined influence of sulphate and temperature on the saturated hydraulic conductivity of hardened cemented paste backfill. *Cem Concr Compos* 8:21–28
- Roshani A, Fall M, Kennedy K (2017) A column study of the hydro-mechanical behavior of mature fine tailings under atmospheric drying. *Intern J Min Sc Technol* 27(2):203–209
- Saiang D, Malmgren L, Nordlund E (2005) Laboratory tests on shotcrete–rock joints in direct shear, tension and compression. *Rock Mech Rock Eng* 38(4):275–297
- Scrivener KL, Crumbie AK, Laugesen P (2004) The interfacial transition zone (ITZ) between cement paste and aggregate in concrete. *Interface Sci* 12(4):411–421
- Seidel JP, Haberfield CM (2002) Theoretical models for concrete–rock joints subjected to constant normal stiffness direct shear. *Int J Rock Mech Min Sci* 39:539–553
- Sha W, O'Neill E, Guo Z (1999) Differential scanning calorimetry study of ordinary Portland cement. *Cem Concr Res* 29(9):1487–1489
- Taylor HFW (1964) *The chemistry of cements*, vol 1. Academic Press, London
- Terzaghi K (1943) *Theoretical soil mechanics*. John Wiley & Sons, New York
- Tse R, Cruden DM (1979) Estimating joint roughness coefficients. *Int J Rock Mech Min Sci* 16(5):303–307
- Wang JA, Wang YX, Gao QJ (2015) Behavior of microcontacts in rock joints under direct shear creep loading. *Int J Rock Mech Min Sci* 78:217–229
- Wang Y, Fall M, Wu A (2016) Initial temperature-dependence of strength development and self-desiccation in cemented paste backfill that contains sodium silicate. *Cement Concr Compos* 67:101–110
- Yang PY, Li L (2015) Investigation of the short-term stress distribution in stopes and drifts backfilled with cemented paste backfill. *Int J Min Sci Tech* 25:721–728
- Yang ZY, Lo SC, Di CC (2001) Reassessing the joint roughness coefficient (JRC) estimation using Z2. *Rock Mech Rock Eng* 34:243–251
- Yilmaz E (2018) Stope depth effect on field behaviour and performance of cemented paste backfills. *Int J Min Reclam Environ* 32(4):273–296

- Yilmaz E, Kesimal A, Ercikdi B (2003) The factors affecting the strength and stability of paste backfill. *Yerbilimleri–Turkish Earth Sci* 28(2):155–169
- Yu XB, Vayssade B (1991) Joint profiles and their roughness parameters. *Int J Rock Mech Min Sci Geo Mech Abstr* 28:333–336
- Xue G, Yilmaz E, Song W, Cao S (2019a) Mechanical, flexural and microstructural properties of cement-tailings matrix composites: effects of fiber type and dosage. *Compos B Eng* 172:131–142
- Xue G, Yilmaz E, Song W, Yilmaz E (2019b) Influence of fiber reinforcement on mechanical behavior and microstructural properties of cemented tailings backfill. *Constr Build Mater* 213:275–285
- Zhou Q, Glasser F (2001) Thermal stability and decomposition mechanisms of ettringite at <120 °C. *Cem Concr Res* 31(9):1333–1339

Publisher's Note Springer Nature remains neutral with regard to jurisdictional claims in published maps and institutional affiliations.